The Kinematic Simulation Study of the Working Device of an Unmanned Bulldozer

Chunming Miao[1], Quancheng Dong[1*], Congfeng Tian[2], Ziyao Xu[1], and Guangxiao Shen[1]

[1]School of Mechanical Engineering, University of Jinan, Jinan, Shandong, 250024, China
[2]Shantui Construction Machinery Co., LTD, Jining, Shandong, 272073, China
*Corresponding author's e-mail: me_dongqc@ujn.edu.cn

Abstract. This paper first conducts a kinematic analysis of the bulldozer's working device, deriving the transformation matrices between each joint and formulating the relationship between the blade's end-effector position and orientation and the joint angles in the Cartesian coordinate system. Next, using a geometric method, the joint space of the working device is converted into the drive space, clarifying the mapping relationship between joint angles and the hydraulic cylinder's extension length. Finally, a simulation model of the working device's linkage mechanism is established, and four sets of joint angles are selected to verify the forward and inverse kinematics analysis. Additionally, a simulation model of the working device's hydraulic system is developed, experimental parameters are set, and the accuracy of the relationship between the joint angles and the hydraulic cylinder's extension length is validated. This provides a theoretical foundation for subsequent research on the operation planning and control of unmanned bulldozer working devices.

Keywords: unmanned bulldozer; working device; kinematic analysis; hydraulic system

1 Introduction

Bulldozers are mainly used to perform tasks such as pushing earth, and filling and leveling the ground in large earthwork projects [1]. In many cases, the operating environment of bulldozers is relatively harsh. For example, when operating in environments such as soil piles, slopes and trenches, problems such as uneven vehicle bodies and excessive load on the blade will be encountered [2]. In harsh environments, it especially tests the skills of drivers. Problems such as construction errors, insufficient construction process data, and low construction efficiency may occur, and construction quality cannot be maintained. Moreover, for drivers, precise construction becomes more difficult, and it is also difficult to effectively protect the safety of drivers. Therefore, intelligent and unmanned bulldozers will become an important development direction in the

future. They will meet the market demand for intelligent bulldozers and have broad prospects and practical application value [3,4]. At present, most research on the automation of earthmoving machinery focuses on excavators, and there is less research on bulldozers.

The working device and its operating system of a bulldozer are the most critical parts of the actual work of a bulldozer. The working device is subject to large amplitude and high-frequency changes in external soil loads. Hence, the driver needs to operate the working device to lift and pitch continuously to change the position of the blade. Therefore, to achieve unmanned operation of the bulldozer's working device, it is necessary to perform position estimation on the working device, match the poses of the bulldozer body and the end of the working device, and then convert the pose information into the length of the hydraulic cylinder. By controlling the elongation and contraction of the hydraulic cylinder, the blade can reach different positions for precise operations and realize unmanned operation of the working device.

In order to realize the control of the working device of the bulldozer, Xue [5] analyzed the kinematics of the dozer by simulation, and Sun [6] studied a sensor fusion algorithm for estimating the attitude of the dozer blade. Through the RTKGPS installed on the bulldozer blade combined with the angle sensor, Kim and Lee et al. [7,8] established a coordinate conversion model, which can obtain the spatial attitude coordinates of the blade through the tablet device.

KOMATSU, a Japanese manufacturer of heavy equipment including excavators and bulldozers, mounted one GNSS sensor on top of a bulldozer cabin, a single IMU (inertial measurement unit) sensor in the cabin, and a stroke sensor in the cylinders for measuring the position and posture of the bulldozer blade. Then, the company manufactured a prototype and verified its performance [9].

As a heavy equipment company, Caterpillar obtains the pitch angle and speed information of the vehicle through the calculation of the least mean-squared estimation [10]. The proposed method can calculate the spatial parameters of the vehicle, which can assist the operator in understanding the vehicle information.

Omelchenko works in the Topcon positioning system. He has proposed a method and device to control the elevation angle and tilt angle of the bulldozer blade [11]. In addition, it is also necessary to analyze the kinematics of the bulldozer and use the homogeneous transformation matrix to estimate the accurate position and attitude of the blade edge.

Lundeen et al. at the University of Michigan in the United States proposed an optical-marker-based estimation method to estimate the end effector pose of an excavator. He attached an optical marker to the boom, arm, and bucket of the excavator and measured the position and direction of the marker in 3D Cartesian space using a camera. Through this, Lundeen estimated and verified the position of the excavator's bucket tip [12].

Guangcun Zhou and others regarded the excavator as a four-degree-of-freedom mechanical arm. After performing a kinematic analysis on its working device, they converted the rotation angles of each part of the excavating arm into the displacements of each hydraulic cylinder in the driving space [13].

At present, in the research on the control of the working devices of construction machinery such as bulldozers and excavators at home and abroad, their working devices

are usually treated as multi-degree-of-freedom mechanical arms to control the end of the working device to track the planned desired trajectory [14]. This paper proposes a positioning method for the working device of an unmanned bulldozer. This method regards the bulldozer as a three-degree-of-freedom mechanical arm. First, we perform a kinematic analysis on the working device of the bulldozer, establish a mathematical model, and use the homogeneous transformation matrix to calculate the pose of the tooth tip at the end of the blade. Then, according to the coordinate information of the key points on the operation path, we perform an inverse kinematic solution to find out the angles at which each joint needs to rotate. Finally, we use the geometric method to convert the joint space and the driving space to find the control quantity, which is convenient for the subsequent unmanned bulldozer to accurately level the working device, meet the operation requirements and improve the operation efficiency.

2 Kinematic Analysis

The structure of the working device of a bulldozer is shown in Figure 1. The working device of a bulldozer is mainly composed of a blade, a push frame, two blade lifting hydraulic cylinders, and two blade pitching hydraulic cylinders. The blade is the most crucial part of the bulldozer's working device. This article will analyze the blade. The movement of the blade is determined by the telescopic movement of the hydraulic cylinder. When the lifting hydraulic cylinder contracts, the blade is lifted. When the hydraulic cylinder extends, the blade descends. This is called the lifting movement of the blade. When the pitching hydraulic cylinder contracts, the blade tilts upward. When the hydraulic cylinder extends, the blade tilts downward. This is called the pitching movement of the blade.

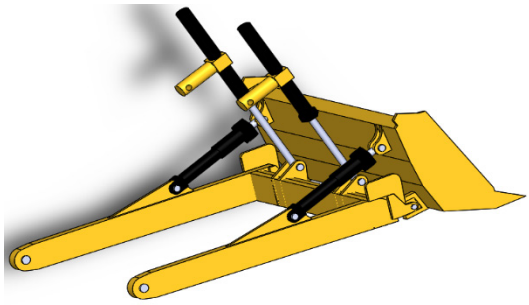

Fig. 1. Structure of the blade.

2.1 Forward Kinematics Solution

From the perspective of robotics, a bulldozer can be regarded as a robotic arm with three degrees of freedom. According to the establishment concept of the Denavit-Hartenberg coordinate system, the direction of the rotating shaft is set as the Z axis, the

direction of the common perpendicular of the two axes is taken as the X axis, and then the Y axis is determined by using the right-hand rule. The rotary coordinate system/base coordinate system, lifting coordinate system, pitching coordinate system, and tooth tip coordinate system are established, respectively, as shown in Figure 2.

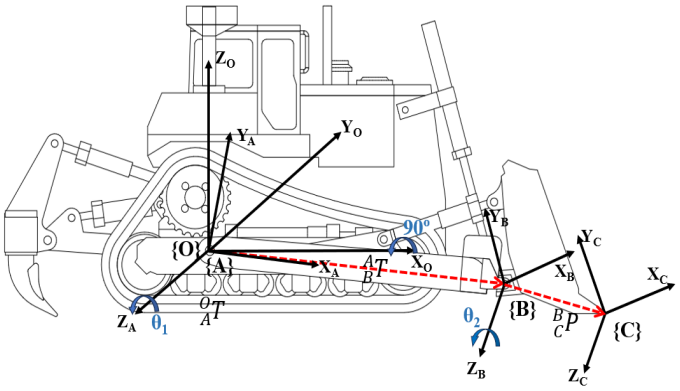

Fig. 2. Coordinate system structure for kinematic analysis of bulldozers.

The coordinate system O{X_O, Y_O, Z_O } is the base coordinate system attached to the center of the bulldozer track. The coordinate system A{X_A, Y_A, Z_A } defines the rotation center of the blade lifting motion. The origins of the base coordinate system {O} and the lifting coordinate system {A} are defined at the same rotation center. The coordinate system B{X_B, Y_B, Z_B } defines the rotation center of the blade pitching motion. The coordinate system C{X_C, Y_C, Z_C } is the coordinate system attached to the tooth tip of the blade. The position where the blade teeth are located is the designed surface required during bulldozer operation. In three-dimensional Cartesian space, the relationship between two adjacent coordinate systems is represented by a homogeneous transformation matrix using Z-Y-R Euler angles. Among them, the relationship between the coordinate systems {O} and {A} is expressed as:

$$ {}^{O}_{A}T = R(x, 90º)\, R(z, \theta_1) = \begin{bmatrix} c\theta_1 & -s\theta_1 & 0 & 0 \\ 0 & 0 & -1 & 0 \\ s\theta_1 & c\theta_1 & 0 & 0 \\ 0 & 0 & 0 & 1 \end{bmatrix} \tag{1} $$

where $c\theta_1 = \cos\theta_1, s\theta_1 = \sin\theta_1$. Here, θ_1 is the angle at which the bulldozer blade is lifted around the Z_A axis. In three-dimensional Cartesian space, the position of the coordinate system {C} attached to the tooth tip of the blade is represented by P_C. We construct a homogeneous transformation matrix for it as follows and calculate its position.

$$ P_C = {}^{O}_{A}T\, {}^{A}_{B}T\, {}^{B}_{C}P = \begin{bmatrix} p_x \\ p_y \\ p_z \\ 1 \end{bmatrix} \tag{2} $$

Since there is both translation and rotation between coordinate system {B} and coordinate system {A}, then,

$$
{}^{A}_{B}T = Trans(x_{ab}, y_{ab}, z_{ab})\, R(z, \theta_2)
$$

$$
= \begin{bmatrix} 1 & 0 & 0 & x_{ab} \\ 0 & 1 & 0 & y_{ab} \\ 0 & 0 & 1 & z_{ab} \\ 0 & 0 & 0 & 1 \end{bmatrix} \begin{bmatrix} c\theta_2 & -s\theta_2 & 0 & 0 \\ s\theta_2 & c\theta_2 & 0 & 0 \\ 0 & 0 & 1 & 0 \\ 0 & 0 & 0 & 1 \end{bmatrix}
$$

$$
= \begin{bmatrix} c\theta_2 & -s\theta_2 & 0 & x_{ab} \\ s\theta_2 & c\theta_2 & 0 & y_{ab} \\ 0 & 0 & 1 & z_{ab} \\ 0 & 0 & 0 & 1 \end{bmatrix} \tag{3}
$$

$$
{}^{B}_{C}P = \begin{bmatrix} l_{bw} \\ l_{bh} \\ 0 \\ 1 \end{bmatrix} \tag{4}
$$

where, $c\theta_2 = \cos\theta_2, s\theta_2 = \sin\theta_2$. Here, θ_2 is the angle at which the bulldozer blade pitches around the Z_B axis. x_{ab}, y_{ab}, and z_{ab} represent the distance from the origin of the pitching coordinate system {B} to the origin of the lifting coordinate system {A}. Since only a translational transformation along the x-axis is performed from coordinate system {A} to coordinate system {B}, x_{ab} is equal to the length l_1 of the bulldozer blade push rod, $y_{ab} = 0, z_{ab} = 0, l_{BW}$ is the thickness of the bulldozer blade, and l_{bh} represents the height difference from the origin of the tooth tip coordinate system {C} to the pitching coordinate system {B}, as shown in Figure 3.

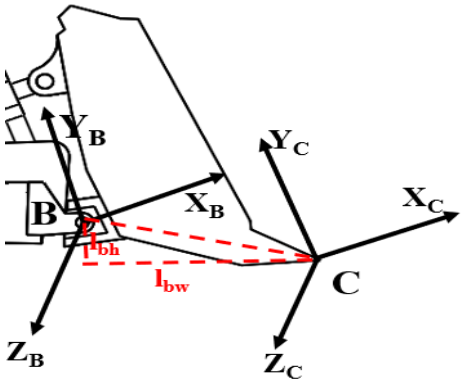

Fig. 3. Dimensions of the blade.

Substituting Equations (1), (3), and (4) into Equation (2) yields:

$$P_C = \begin{bmatrix} p_x \\ p_y \\ p_z \\ 1 \end{bmatrix}$$

$$\begin{cases} p_x = l_{bw}(c\theta_1 c\theta_2 - s\theta_1 s\theta_2) - l_{bh}(c\theta_1 s\theta_2 + s\theta_1 c\theta_2) \\ \quad +x_{ab}c\theta_1 - y_{ab}s\theta_1 \\ \quad p_y = -z_{ab} \\ p_z = l_{bw}(s\theta_1 c\theta_2 - s\theta_1 s\theta_2) - l_{bh}(s\theta_1 s\theta_2 - c\theta_1 c\theta_2) \\ \quad +x_{ab}s\theta_1 + y_{ab}c\theta_1 \end{cases} \tag{5}$$

The obtained P_C is the position and orientation information of the tooth tip at the end of the blade in the base coordinate system of the bulldozer.

2.2 Inverse Kinematics Solution

The above forward kinematics solution is to obtain the position and orientation information of the tooth tip at the end of the blade in the base coordinate system under the condition that the rotation angles of each joint are known. However, if we want to control the bulldozer blade to complete various pose tasks without human operation, inverse kinematics needs to be performed to obtain the rotation angles of each joint in the joint space. The process of solving the inverse kinematics of the blade is as follows:

$$P_C = {}^{O}_{A}T\,{}^{A}_{B}T\,{}^{B}_{C}P = \begin{bmatrix} p_x \\ p_y \\ p_z \\ 1 \end{bmatrix}, ({}^{O}_{A}T)^{-1} = \begin{bmatrix} c\theta_1 & 0 & s\theta_1 & 0 \\ -s\theta_1 & 0 & c\theta_1 & 0 \\ 0 & -1 & 0 & 0 \\ 0 & 0 & 0 & 1 \end{bmatrix}$$

Multiplying this equation obtains:

$$({}^{O}_{A}T)^{-1}P_C = ({}^{O}_{A}T)^{-1}\,{}^{O}_{A}T\,{}^{A}_{B}T\,{}^{B}_{C}P$$

$$\begin{bmatrix} c\theta_1 & 0 & s\theta_1 & 0 \\ -s\theta_1 & 0 & c\theta_1 & 0 \\ 0 & -1 & 0 & 0 \\ 0 & 0 & 0 & 1 \end{bmatrix} \begin{bmatrix} p_x \\ p_y \\ p_z \\ 1 \end{bmatrix} = \begin{bmatrix} c\theta_2 & -s\theta_2 & 0 & x_{ab} \\ s\theta_2 & c\theta_2 & 0 & y_{ab} \\ 0 & 0 & 1 & z_{ab} \\ 0 & 0 & 0 & 1 \end{bmatrix} \begin{bmatrix} l_{bw} \\ l_{bh} \\ 0 \\ 1 \end{bmatrix}$$

$$\begin{bmatrix} p_x c\theta_1 + p_z s\theta_1 \\ -p_x s\theta_1 + p_z c\theta_1 \\ -p_y \\ 1 \end{bmatrix} = \begin{bmatrix} l_{bw}c\theta_2 - l_{bh}s\theta_2 + x_{ab} \\ l_{bw}s\theta_2 + l_{bh}c\theta_2 + y_{ab} \\ z_{ab} \\ 1 \end{bmatrix}$$

The corresponding parts on both sides of the equation are equal, and we obtain.

$$p_x c\theta_1 + p_z s\theta_1 = l_{bw}c\theta_2 - l_{bh}s\theta_2 + x_{ab} \tag{6}$$

$$-p_x s\theta_1 + p_z c\theta_1 = l_{bw} s\theta_2 + l_{bh} c\theta_2 + y_{ab} - p_y = z_{ab} = 0 \quad (7)$$

First, we multiply Equation (6) by p_z and multiply Equation (7) by p_x. Then, we subtract the two equations.

$$\begin{aligned} &p_z\,(p_x c\theta_1 + p_z s\theta_1) - p_x\,(-p_x s\theta_1 + p_z c\theta_1) \\ &= p_z\,(l_{bw} c\theta_2 - l_{bh} s\theta_2 + x_{ab}) - p_x\,(l_{bw} s\theta_2 + l_{bh} c\theta_2 + y_{ab}) \end{aligned}$$

Simplifying the above equation gives:

$$\left({p_x}^2 + {p_y}^2\right) s\theta_1 = \&(p_z l_{bw} - p_x l_{bh}) c\theta_2 - (p_z l_{bh} + p_x l_{bw}) s\theta_2 + x_{ab} p_z - y_{ab} p_x \quad (8)$$

We multiply Equation (6) by p_x and multiply Equation (7) by p_z. Then, we add the two equations.

$$\begin{aligned} \left({p_x}^2 + {p_y}^2\right) c\theta_1 = (p_x l_{bw} + p_z l_{bh}) c\theta_2 + (p_z l_{bw} - p_x l_{bh}) s\theta_2 \\ + x_{ab} p_x + y_{ab} p_z \end{aligned} \quad (9)$$

Then, we divide Equation (8) by Equation (9) to obtain the expression of θ_1:

$$tan\theta_1 =$$

$$\frac{(p_z l_{bw} - p_x l_{bh}) c\theta_2 - (p_z l_{bh} + p_x l_{bw}) s\theta_2 + x_{ab} p_z - y_{ab} p_x}{(p_x l_{bw} + p_z l_{bh}) c\theta_2 + (p_z l_{bw} - p_x l_{bh}) s\theta_2 + x_{ab} p_x + y_{ab} p_z}$$

$$\begin{aligned} \theta_1 = \arctan\{&[(p_z l_{bw} - p_x l_{bh}) c\theta_2 - (p_z l_{bh} + p_x l_{bw}) s\theta_2 + x_{ab} p_z - \\ &y_{ab} p_x]/[(p_z l_{bw} - p_x l_{bh}) c\theta_2 - (p_z l_{bh} + p_x l_{bw}) s\theta_2 + x_{ab} p_z - y_{ab} p_x]\} \end{aligned} \quad (10)$$

Substituting θ_1 into the original Equation (6) and simplifying, we obtain the expression of θ_2:

$$\begin{aligned} \theta_2 = \arctan\{&{l_{bw}}^2 - {l_{bh}}^2 + {p_x}^2 + {p_z}^2 + {x_{ab}}^2 + {y_{ab}}^2 - [({l_{bw}}^2 - {l_{bh}}^2 + {l_{bw}}^2 + \\ &{p_z}^2)^2 + 4(p_z\, l_{bw} - p_x\, l_{bh})(p_x\, l_{bw} + p_z\, l_{bh})]^{\frac{1}{2}}/({l_{bw}}^2 - {l_{bh}}^2 + {p_x}^2 + {p_z}^2)\} \end{aligned} \quad (11)$$

Since the equation about θ_1 in Equation (10) contains θ_2, then we substitute Equation (11) into Equation (6) again and simplify to obtain:

$$\theta_1 = \arctan\left[\frac{(p_x l_{bw} + p_z l_{bh})}{(p_z l_{bw} - p_x l_{bh})}\right] \quad (12)$$

By using this method, the coordinate points on the bulldozer's operation path can be converted into the coordinates of the tooth tip at the end of the blade, and then the joint angles of the blade in the joint space can be solved inversely. The steps are shown in Figure 4.

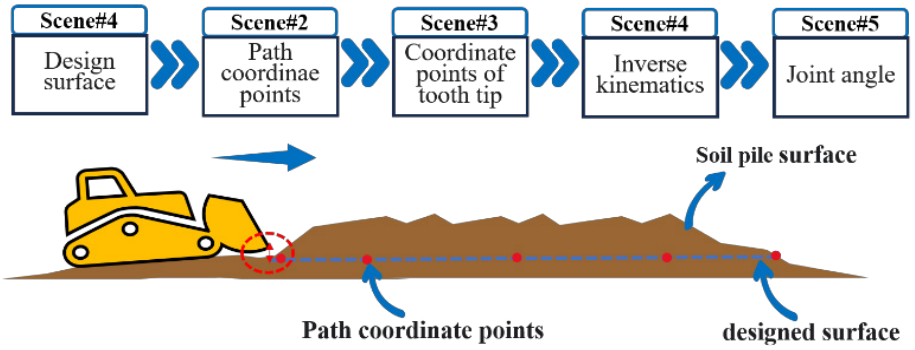

Fig. 4. Inverse solution steps.

3 Conversion between Joint Space and Actuation Space

The result obtained from the forward kinematics solution of the bulldozer blade, as mentioned above, is the description of the tooth tip at the end of the blade in the pose space. The result obtained from the inverse kinematics solution is the rotation angle of the blade in the joint space. However, to realize the operation planning and control of the unmanned bulldozer blade, it is also necessary to realize the mutual conversion between the joint angle of the bulldozer blade and the length of the hydraulic cylinder, that is, the conversion between the joint space and the actuation space of the blade.

As can be seen from the structure of the bulldozer, the positions of the hinge points between the working device hydraulic cylinder and the vehicle body are fixed, the lengths and tilt angles of the connecting lines between each hinge point are fixed, and the structure is relatively simple. Therefore, the geometric method is selected to complete the conversion between the joint space and the driving space.

3.1 Conversion between lifting Angle and Stroke of Lifting Hydraulic Cylinder

As shown in Figure 5, it is a structural schematic diagram of the hinge points of each joint when the bulldozer blade is lifted. Point O is the hinge point between the top push rod and the center of the bulldozer track. Point A is the hinge point between the blade of the bulldozer blade and the top push rod. Point C is the hinge point between the support rod of the lifting hydraulic cylinder and the bulldozer body. AO, CO, BC, and $\angle$ABC are all known quantities, and the length of AO is equal to the length of the top push rod. AB is the length λ_1 of the lifting hydraulic cylinder to be found.

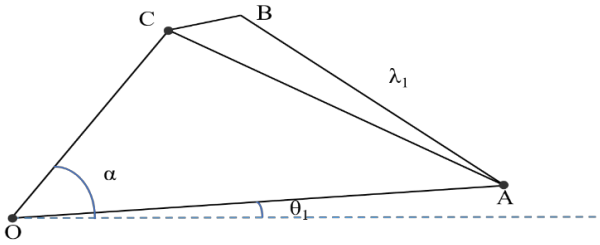

Fig. 5. Structural schematic diagram of lifting process.

In ΔAOC, it can be obtained by the cosine theorem:

$$AC = \sqrt{AO^2 + CO^2 - 2AO\ CO\ \cos\angle AOC} \tag{13}$$

$$\angle \mathrm{AOC} = \alpha \pm \theta_1 \tag{14}$$

In the formula, α is the angle between OC and the horizontal plane, which is a constant value. θ_1 can be obtained by the above inverse kinematics solution.

Similarly, in ΔABC,

$$AB = \sqrt{AC^2 - BC^2 + 2AB\ BC\ \cos\angle ABC} \tag{15}$$

By combining Equations (13), (14) and (15), the conversion formula between the lifting angle θ_1 of the bulldozer blade and the length λ_1 of the lifting hydraulic cylinder can be obtained as:

$$\lambda_1 = AB = [AO^2 + CO^2 - BC^2\ + 2AB\ BC\cos\angle ABC - 2AO\ CO\cos(\alpha \pm \theta_1)]^{\frac{1}{2}} \tag{16}$$

3.2 Conversion between Pitch Angle and Stroke of Pitch Hydraulic Cylinder

As shown in Figure 6, it is a structural schematic diagram of the hinge points of each joint when the bulldozer blade pitches. E is the fixed point of the pitch hydraulic cylinder and the top push rod, and F is the fixed point of the hydraulic cylinder and the bulldozer blade. In the figure, θ_2 is obtained by inverse kinematics solution. AE and AF are both known quantities. EF is the length λ_2 of the pitch hydraulic cylinder to be found.

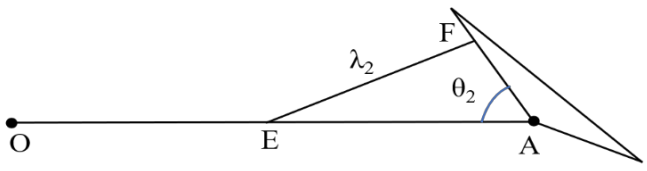

Fig. 6. Structural diagram of the pitching process.

In ΔAEF, the conversion formula between the pitch angle θ_2 of the bulldozer blade and the length λ_2 of the pitch hydraulic cylinder can be obtained by the cosine theorem as follows:

$$\lambda_2 = EF = \sqrt{AE^2 + AF^2 - 2AE\ AF\ \cos\theta_2} \tag{17}$$

After the above calculations, the joint space and actuation space of the blade are converted, and the mapping relationship between each joint angle and the elongation of the lifting and pitching hydraulic cylinders is clarified. Then, by controlling the elongation and contraction of the hydraulic cylinders, the tooth tip at the end of the bulldozer blade reaches the path points on the design surface of the operation task to complete the operation task.

4 Simulation Verification.

4.1 Forward Kinematics Simulation

The bulldozer is regarded as a robot with three degrees of freedom and can be simplified into a three-link mechanism, as shown in Figure 7. Since the base coordinate of the bulldozer coincides with the origin of the lifting coordinate system, the length of the first link is set to 0 mm. The length of the second link is the length of the top push frame l_1, which is set to 2050 mm. The length of the third link is the thickness of the blade, which is set to 600 mm.

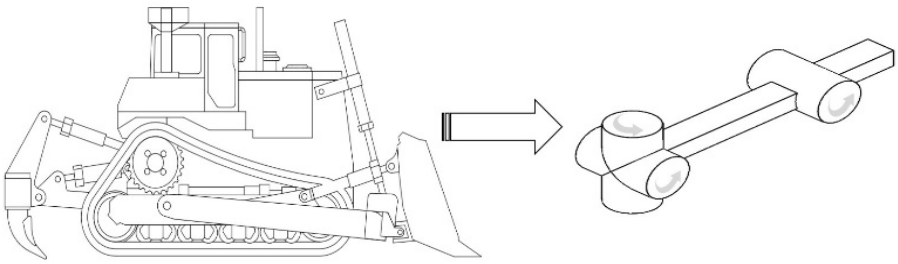

Fig. 7. The bulldozer is simplified into a three-link mechanism.

In this section, the Toolbox will be used to verify the forward and inverse kinematics equations derived to check their correctness.

In forward kinematics, the angles θ_1 and θ_2 and the distance l_1 are known, while the position of the blade is unknown. As can be seen from the content in Section 2, θ_1 is the lifting angle of the blade, θ_2 is the pitch angle of the blade, and the distance l_1 is the length of the top push frame which is 2050mm. The pose of the tooth tip at the end of the blade is represented by the matrix $P_C = (p_x, p_y, p_z)$.

Therefore, in the Toolbox, four sets of joint angle parameters $\theta_{group1} \sim \theta_{group4}$ are set. Each set of joint angles contains the yaw angle θ_0 of the bulldozer, the lifting angle

θ_1 of the blade, and the pitch angle θ_2. This experiment mainly focuses on the lower-level blade movement. Kinematic constraints are applied to the model. The degrees of freedom of the blade are limited to the movements of the X and Z axes. Only the joint angles θ_1 and θ_2 of the blade are considered, while the yaw angle θ_0 of the bulldozer is not considered. Therefore, the yaw angle θ_0 of the bulldozer is uniformly set to 0°.

Next, the Toolbox is used to perform forward kinematics simulation on the blade. We set the link lengths in the Toolbox, draw the three-link mechanism model of the blade, and then set four different sets of joint angles to obtain four different poses of the blade, as shown in Figure 8.

Then, by substituting four different sets of joint angles into the forward kinematics equation derived in Section 2 for calculation, we compared the pose coordinates of the blade tip calculated by the two methods to verify whether the forward motion analysis is correct. The results are shown in Table 1.

It can be concluded from the data in Table 1 that the pose coordinates of the end of the blade calculated by the forward kinematics equation derived in Chapter 2 are the same as the results obtained by simulation calculation in the Toolbox. Through the verification of calculation by kinematics equation and simulation calculation, it can be seen that the model of the blade is established correctly. Therefore, the forward kinematics analysis of this model is accurate.

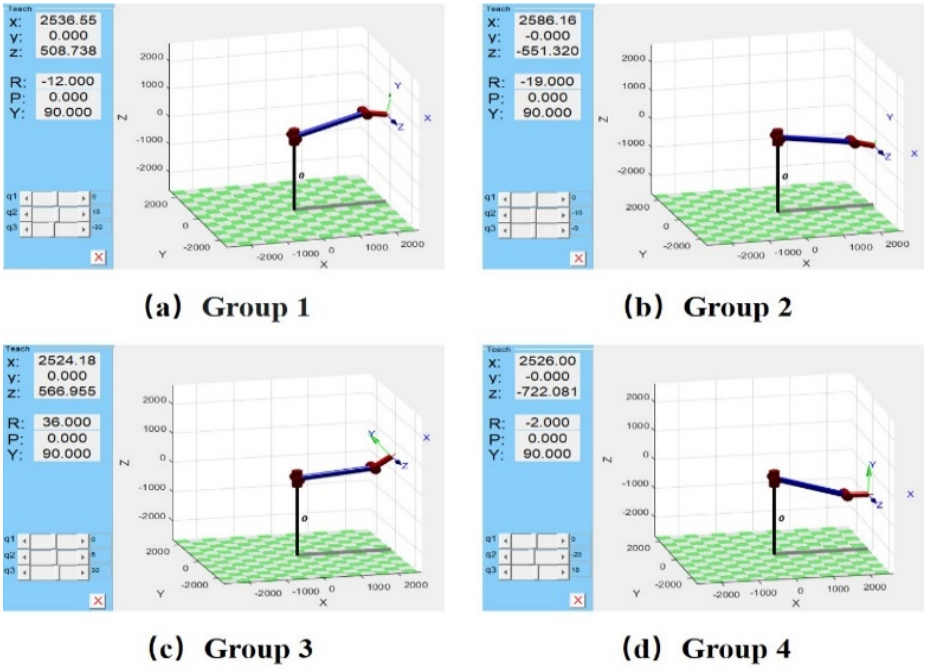

Fig. 8. Blade poses under four sets of joint angles.

Table 1. Pose coordinates of the end of the blade obtained by different methods.

joint angle (°)	value-taking method	Pose coordinates of the end of the blade(mm)		
		p_x	p_y	p_z
θ_{group1}=[0,18,-30]	Calculation by forward kinematics equation	2536.554	0.000	508.738
	Toolbox simulation	2536.554	0.000	508.738
θ_{group1}=[0,-10,-9]	Calculation by forward kinematics equation	2586.167	0.000	-551.320
	Toolbox simulation	2586.167	0.000	-551.320
θ_{group1}=[0,6,30]	Calculation by forward kinematics equation	2524.180	0.000	566.955
	Toolbox simulation	2524.180	0.000	566.955
θ_{group1}=[0,-20,18]	Calculation by forward kinematics equation	2526.004	0.000	-722.081
	Toolbox simulation	2526.004	0.000	-722.081

4.2 Inverse Kinematics Simulation

The inverse kinematics simulation is carried out by using the ikine() inverse kinematics solution function in the Toolbox. The pose matrices P_{C_1} ~ P_{C_4} of the tooth tips at the end of the blade obtained by the forward kinematics solution are brought into the ikine() function, and the corresponding joint angles q_1~q_4 are obtained by simulation. There are multiple sets of solutions for the joint angles obtained by this inverse kinematics solution. We select a set of solutions with the same angles as in Table 1. The results are shown in Table 2. q_1 ~ q_4 in Table 2 are the radian representation forms of the joint angles obtained by the Toolbox. After this result is converted into angles, it is the same as the joint angles set in Table 1, which further proves the correctness of the modeling.

In conclusion, this analysis is correct.

Table 2. Inverse kinematics calculation results.

End pose matrix	Calculation result
$P_{C_1} = \begin{bmatrix} 2536.554 \\ 0.000 \\ 508.738 \end{bmatrix}$	$q_1 = [0.000 \quad 0.314 \quad -0.524]$
$P_{C_2} = \begin{bmatrix} 2586.167 \\ 0.000 \\ -551.320 \end{bmatrix}$	$q_2 = [0.000 \quad -0.175 \quad -0.157]$

$P_{C_3} = \begin{bmatrix} 2524.180 \\ 0.000 \\ 566.955 \end{bmatrix}$	$q_3 = [0.000 \quad 0.105 \quad 0.524]$
$P_{C_4} = \begin{bmatrix} 2526.004 \\ 0.000 \\ -722.081 \end{bmatrix}$	$q_4 = [0.000 \quad -0.349 \quad 0.314]$

4.3 Simulation of Drive Space

In Section 2, the mapping relationship between the joint rotation angle of the blade and the stroke of the hydraulic cylinder is calculated by using the geometric method. In this section, the hydraulic component library and 2D mechanical library in Amesim will be jointly used to establish a simulation model to verify the accuracy of its mapping relationship.

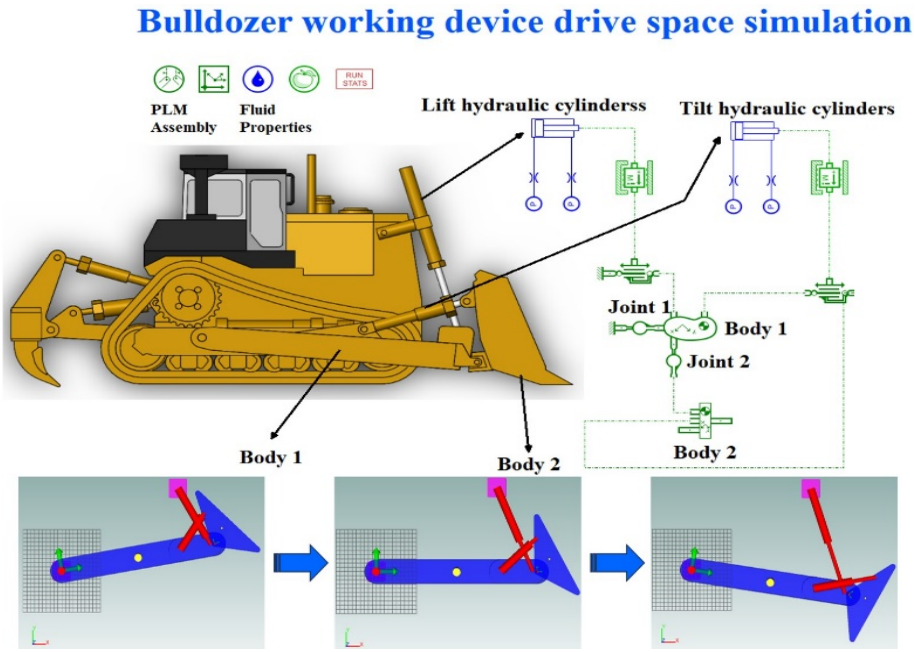

Fig. 9. Structural block diagram of the combined simulation of the bulldozer blade.

Figure 9 shows the structural block diagram of the simulation. Since the lifting hydraulic cylinders of the bulldozer are symmetrically distributed on both sides of the blade and the stroke changes of the two hydraulic cylinders are the same, the two symmetrical hydraulic cylinders can be simplified into one hydraulic cylinder. By the same token, the two-pitch hydraulic cylinders can also be simplified into one. The bulldozer's pusher frame is set as Body1, and the blade is set as Body2. In the process of modeling, this experiment adopts the method of relative coordinate system. According to the

actual size of the bulldozer, input the center of gravity coordinates and masses of the two entities, the coordinate values of each hinge point, and the cylinder diameter, piston rod diameter, stroke, oil pressure and other parameters of the two hydraulic cylinders. Here only the important parameters are explained: lifting hydraulic cylinder diameter: 100mm, rod diameter: 80mm, stroke: 1100mm; the coordinate value of the origin of the blade (Body2) relative coordinate system in the absolute coordinate system: (4,0), and the hinge point with the pusher frame (Body1) is located at the origin of the relative coordinate system, center of gravity coordinates: (0.3,0.3), the coordinate of the tooth tip at the end of the blade: (1,-0.5), mass: 50kg.

Finally, we set the oil pressure in the rod chamber and the rodless chamber of the lifting and pitching hydraulic cylinders, followed by a simulation experiment. The obtained corner curves of each joint are shown in Figure 10-a. Among them, the yellow curve represents the lifting angle θ_1, and the green curve represents the pitching angle θ_2. The stroke change curves of each hydraulic cylinder are shown in Figure 10-b. Among them, the red curve represents the extension length of the lifting hydraulic cylinder, and the blue curve represents the extension length of the pitching hydraulic cylinder.

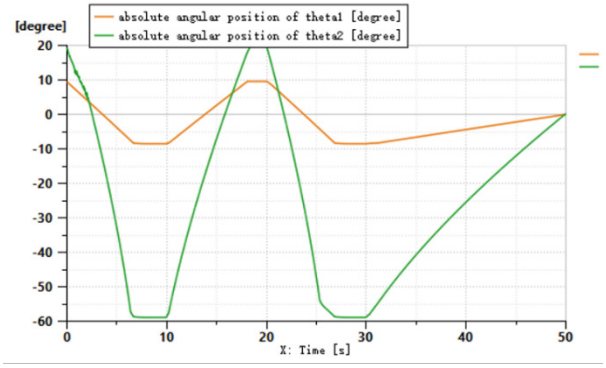

(a)Curves of rotation angles of each joint

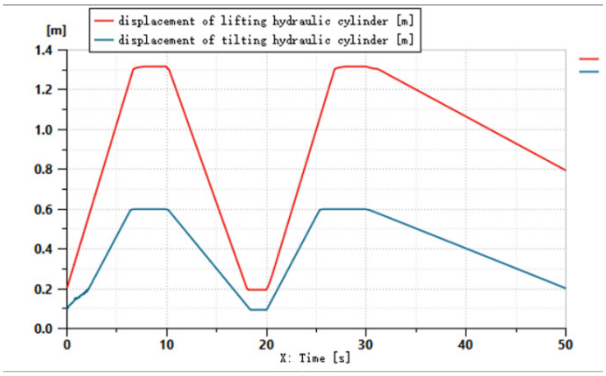

(b)Stroke curves of each hydraulic cylinder

Fig. 10. Simulation curves under different poses of the blade.

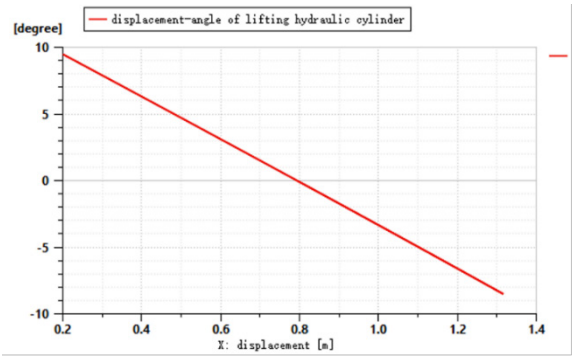

(c)Conversion relationship between lifting hydraulic cylinder and lifting angle

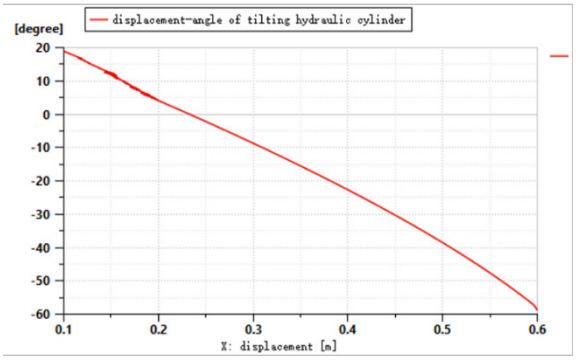

(d)Conversion relationship between tilting hydraulic cylinder and tilting angle

Fig. 11. Conversion relationship between each joint space and drive space.

According to the curves in Figure 10, it can be seen that at the initial position, the lifting angle of the blade is 10°, and at this time, the lifting hydraulic cylinder extends by 0.2m; the pitching angle is 20°, and the pitching hydraulic cylinder extends by 0.1m. At 10s and 30s, the blade drops by -9°, the blade pitches by -60°, and the distances extended by the lifting and pitching hydraulic cylinders are the longest, which are 1.3m and 0.6m, respectively. Finally, the blade stops at a horizontal position. At this time, the rotation angles of each joint are all 0°, the lifting hydraulic cylinder extends by 0.8m, and the pitching hydraulic cylinder extends by 0.2m. We convert the results in Figure 10 into curves in the style of Figure 11, where the abscissa is the stroke, and the ordinate is the joint angle. From the curve in Figure 11, it can be intuitively seen that the relationship between the joint angle and the hydraulic cylinder stroke is approximately linear. Finally, substituting the points on the curve in Figure 11 into the conversion formula of the joint angle and hydraulic cylinder stroke obtained by the geometric method in Section 2 can verify the accuracy of the mapping relationship between the joint space of the blade and the drive space.

5 Conclusions

From the perspective of robotics, this paper simplifies the unmanned bulldozer into a three-degree-of-freedom linkage mechanism, establishes the coordinate system of each joint according to the Denavit-Hartenberg parameter method, and solves the forward and inverse kinematics. The Toolbox is used to solve the attitude of the tooth tip at the end of the bulldozer blade, as well as the rotation angles of each joint. The comparison verifies that the theoretical analysis is correct. Finally, the rotation angles of each joint of the bulldozer blade are converted into the change of the stroke of each hydraulic cylinder. The Amesim software is used to establish a simulation model for the hydraulic cylinder and the blade entity to verify the accuracy of the mapping relationship between the joint space of the blade and the drive space, providing theoretical support for the subsequent research on operation planning and control of related unmanned bulldozer blades.

Acknowledgment

This work was financially supported by the Key R&D project of Shandong Province (2019JZZY010443) fund.

References

1. Huang, Z.Y., Chen, M.(2007) Some new structures and new technologies of crawler bulldozers. Construction Machinery, (3).
2. Sun Q, Bai S, Li G, et al. Modeling and simulation of power transmission of crawler bulldozer[J].Transactions of the Chinese Society of Agricultural Engineering,2018, volume 28:57-61(5).
3. Wang H, Sun F C. Dynamic Modeling and Simulation on a Hybrid Power System for Dual-Motor-Drive Electric Tracked Bulldozer[J].Applied Mechanics&Materials,2014, 494-495:229-233.
4. Guo, G., Gong, L.H. (1998) Research on fuzzy control of cutting depth of bulldozer blade. Construction Machinery, (12): 13-15.
5. Gang Xue, C. S. Han, Y. S. Lee, C.U.Ji, M. S. Kang. "A study on the kinematic analysis and dynamic simulation for automatic 3D control of the dozer blade." Conference paper of KSPE, (2015.5): 419-420.
6. D. I. Sun, C. S. Han, Y. S. Lee, S. H. Kim, S. H. Lee. "A Study on Sensor Fusion Algorithm for Dozer's Blade Position and Attitude Estimation." Conference paper of KSPE, (2016.5): 47-48.
7. S.H. Kim, Y.S. Lee, D.I. Sun, et al., Development of bulldozer sensor system for estimating the position of blade cutting edge, Autom. Constr. 106 (Oct) (2019) 102890.1–102890.11.
8. Y.S. Lee, S.H. Kim, J. Seo, et al., Blade control in Cartesian space for leveling work by a bulldozer, Autom. Constr. 118 (2020) 103264.
9. Komatsu Corporation, Intelligent Machine Control, On-line: https://www.komatsu.eu/en/Komatsu-Intelligent-Machine-Control , Accessed date: 27 February 2019.

10. G. Jayaraman, K.L. Stratton, E.F. Lee, K.W. Kleimenhagen, H.J. Chizeck, Method and apparatus for determining pitch and ground speed of an earth moving machines, in: U.S. Patent No. 5,860,480, 19 Jan, 1999 doi: US5860480.
11. Omelchenko, A., and Zhdanov, A. V. Automatic blade control system with integrated global navigation satellite system and inertial sensors, U.S. Patent No. 8, 145,391, 27 Mar, 2012.
12. K.M. Lundeen, S. Dong, N. Fredricks, M. Akula, J. Seo, V0.R. Kamat, Optical marker-based end effector pose estimation for articulated excavators, Autom. Constr. 65 (2016) 51–64, https://doi.org/10.1016/j.autcon.2016.02.003.
13. Zhou, G.C.(2021) Research on autonomous operation planning and control of excavators. https://kns.cnki.net/kcms2/article.
14. He, Q.H., Chen, M.(2006) Simulation research on a working device of hydraulic excavator. J. Journal of System Simulation,(03):735-738+746.